Geophysical Research Letters

RESEARCH LETTER
10.1029/2020GL089396

Oceanic Processes in Ocean Temperature Products Key to a Realistic Presentation of Positive Indian Ocean Dipole Nonlinearity

Kai Yang[1,2,3], Wenju Cai[4,3], Gang Huang[1], Guojian Wang[4,3], Benjamin Ng[3], and Shujun Li[4,3]

[1]State Key Laboratory of Numerical Modeling for Atmospheric Sciences and Geophysical Fluid Dynamics, Institute of Atmospheric Physics, Chinese Academy of Sciences, Beijing, China, [2]Key Laboratory of Meteorological Disaster, Ministry of Education and Collaborative Innovation Center on Forecast and Evaluation of Meteorological Disasters, Nanjing University of Information Science and Technology, Nanjing, China, [3]Center for Southern Hemisphere Oceans Research (CSHOR), CSIRO Oceans and Atmosphere, Hobart, Australia, [4]Key Laboratory of Physical Oceanography–Institute for Advanced Ocean Studies, Ocean University of China and Qingdao National Laboratory for Marine Science and Technology, Qingdao, China

Key Points:
- Characteristics of extreme positive Indian Ocean Dipole events differ vastly among ocean temperature products
- Nonlinear zonal and vertical advection along the equatorial Indian Ocean contributes to the strong differences
- Involvement of an oceanic model in ocean temperature reconstructions improves representation of the nonlinearity

Supporting Information:
- Supporting Information S1

Correspondence to:
W. Cai,
wenju.cai@csiro.au

Citation:
Yang, K., Cai, W., Huang, G., Wang, G., Ng, B., & Li, S. (2020). Oceanic processes in ocean temperature products key to a realistic presentation of positive Indian Ocean Dipole nonlinearity. *Geophysical Research Letters*, *46*, e2020GL089396. https://doi.org/10.1029/2020GL089396

Received 20 JUN 2020
Accepted 31 JUL 2020
Accepted article online 4 AUG 2020

Abstract A positive Indian Ocean Dipole (pIOD) refers to a sea surface temperature anomaly pattern with cold anomalies in the equatorial eastern Indian Ocean and warm anomalies in the west, leading to floods in the eastern African countries and droughts and bushfires in Indonesia and Australia. The pIOD displays strong inter-event differences, ranging from an extreme event dominated by westward-extended strong cold anomalies along the equator, to a moderate event with weakened cooling confined to region off Sumatra-Java. Representation of the extreme pIOD varies vastly across ocean temperature products. Here we show that products generated in a system explicitly involving subsurface oceanic processes capture the nonlinear dynamics of the extreme pIOD, i.e., the equatorial nonlinear zonal and vertical advection, and systematically produce a more realistic extreme pIOD. Thus, our study identifies ocean temperature products that are more suitable for studying extreme pIOD and its climatic impacts.

Plain Language Summary A positive Indian Ocean Dipole (pIOD), with warm and cold sea surface temperature anomalies in the western and eastern equatorial Indian Ocean, respectively, exerts a pronounced impact on the climate extremes, including floods in the eastern African countries and droughts and bushfires in Indonesia and Australia. However, pIOD events vary vastly in amplitude and spatial pattern from one event to another, ranging from extreme events dominated by westward-extended strong cold anomalies along the equator, to moderate events with weakened cooling confined to region off Sumatra-Java. Any product must realistically represent the inter-event difference, because impacts of the extreme and moderate events are rather different. Here we find that ocean temperature products that explicitly involve oceanic processes, in particular, the equatorial oceanic nonlinear zonal and vertical advection, in their construction produce marked pIOD inter-event differences, particularly a greater amplitude of extreme pIODs, than in products that do not. Thus, ocean temperature products that involve oceanic processes are more advantageous for use in pIOD research.

1. Introduction

A positive Indian Ocean Dipole (pIOD) event, which usually peaks in austral spring (September-October-November, SON; Saji et al., 1999), features cold sea surface temperature (SST) anomalies over the eastern equatorial Indian Ocean (EEIO) but warm SST anomalies in the west. Accompanied by easterly wind anomalies along the equator and a westward shift of atmospheric convection to the western Indian Ocean, pIOD events have enormous impacts on climate extremes over the Indian Ocean-rim regions, including devastating droughts and bushfires in Indonesia and Australia, and severe floods in East Africa (Ashok et al., 2003; Behera et al., 2005; Cai et al., 2009; Ummenhofer et al., 2009).

During a developing phase (austral winter) of the pIOD event, an anomalous cooling emerges off Sumatra-Java. The initial cooling is in turn reinforced by the anomalous southeasterlies including anomalous monsoonal winds, and the associated upwelling, in a positive feedback process. The cooling increases the

zonal SST gradient over the tropical Indian Ocean, which in turn promotes easterly anomalies along the equator, intensifying the SST gradient through the positive Bjerknes feedback (Bjerknes, 1969; Saji et al., 1999; Webster et al., 1999). In some extreme pIOD events, the easterlies are particularly strong, further strengthening the SST gradient by cooling the EEIO through the generation of equatorial upwelling Kelvin waves, enhancing evaporation while weakening the eastward heat transport of mean oceanic flows, and warming the western equatorial Indian Ocean (Cai et al., 2014; Feng & Meyers, 2003; Murtugudde et al., 2000; Yu & Rienecker, 1999).

The IOD is conventionally described by a dipole mode index (DMI), calculated as the SST differences between the west (50–70°E, 10°S–10°N) and the east (90–110°E, 10°S–0°N) tropical Indian Ocean (Saji et al., 1999). However, the pIOD has different flavors and nonlinear properties, suggesting that the DMI may not fully capture the characteristics of pIOD (Anil et al., 2016; Cai et al., 2014, 2018; Du et al., 2013; Endo & Tozuka, 2016; Wang et al., 2017). Based on the first and second principal components (PC1 and PC2) of the empirical orthogonal function (EOF) of tropical SON rainfall, Cai et al. (2014) identified a nonlinear relationship between two PCs that distinguish extreme from moderate pIODs. Classification of extreme and moderate pIODs is crucial in order to better understand inter-event differences and their associated physical processes and impacts (Cai et al., 2018; Wang et al., 2017). Extreme pIOD events, like in 1997 and 2019 (Wang et al., 2020), are dominated by nonlinear zonal and vertical advection. They feature strong and westward-extended cold anomalies along the equator and anomalous equatorial easterlies over the eastern Indian Ocean and exert severe impacts in surrounding areas (Abram et al., 2003; Cai et al., 2014; Page et al., 2002).

Although there are many observation-based ocean temperature products available, the IOD properties between different products show a large discrepancy, even using the DMI (Verdon-Kidd, 2018). In this study, we examine the nonlinear characteristics of the pIOD in seven ocean temperature products, including three products generated with an ocean model and four products without an ocean model. The outcome is a recommendation of more suitable products for studying extreme pIOD.

2. Data and Methods

We examine pIOD in seven ocean temperature products. The first is OISST (NOAA Optimum Interpolation SST version 2, Reynolds et al., 2002). Based on satellite products and in situ data from ships and buoys, OISST is constructed weekly using an objective analysis method called Optimum Interpolation with a horizontal resolution of 1° × 1° starting from 1982. This product faithfully assimilates the available observations at a high temporal resolution; therefore, the presence of high variability of the IOD and strong nonlinearity underscores these properties of the pIOD that exist in the real world. As such, this product is regarded as most accurate and truthful to the observations.

Three of the products that explicitly involve an ocean model in their construction are discussed below.

ORA-S5 (European Center for Medium-Range Weather Forecasts Ocean ReAnalysis System 5; Zuo et al., 2019): a historical reconstruction of the ocean and sea-ice state built on the ECMWF operational ocean and sea-ice ensemble reanalysis-analysis system OCEAN5, including five ensemble members (the member used in this study is named "opa0" with a resolution of 1° × 1°) and starting from 1979. Except using an ocean model with a horizontal resolution approximately 25 km in the tropics and 75 vertical levels, ORA-S5 also assimilates an in-situ temperature and salinity data set named EN4, which includes all conventional oceanic observations like Argo, moored buoys, and ship measurements.

SODA (Simple Ocean Data Assimilation version 3.3.1, Carton et al., 2018): a reanalysis based on the Modular Ocean Model (MOM) version 5, with a horizontal resolution of 0.5° × 0.5° and a vertical resolution of 50-levels. SODA 3.3.1 is forced by Modern-Era Retrospective analysis for Research and Applications Version 2, covering the period of 1980–2015. The observations used in SODA include the World Ocean Database of historical hydrographic profiles, in-situ SST from the International Comprehensive Ocean-Atmosphere Data Set (ICOADS), and satellite data. In this study, the potential temperature at 5 m is used to represent the SST.

GODAS (National Centers for Environmental Prediction Global Ocean Data Assimilation System; Behringer & Xue, 2004): a reanalysis based on a quasi-global configuration of the MOM Version 3 with a horizontal resolution of 1° × 1°, enhanced to 1/3° in latitude within 10° of the equator, and 40 vertical levels,

beginning from 1980. GODAS has assimilated observations from the Tropical Atmosphere Ocean (TAO) TRITON and PIRATA mooring and Argo profiling floats etc. In this study, the potential temperature at 5 m is used to represent the SST.

The three products that do not involve an ocean model in their construction are listed below.

COBESST (Centennial In Situ Observation Based Estimates of the Variability of SST and Marine Meteorological Variables, SST2; Hirahara et al., 2013): a centennial scale ocean temperature product with a horizontal resolution of 1° × 1° starting from 1850. Combining SST from ICOADS and the Japanese Kobe collection etc., COBESST is constructed as the sum of secular trend, interannual variations, and daily changes. The secular trend and interannual variations are reconstructed based on EOF analysis, and daily changes are analyzed using observation during the day of the analysis. Satellite observations are used for constructing interannual SST variations and are not used in the final product.

ERSST (Extended Reconstructed Sea Surface Temperature Version 3b; Smith et al., 2008): an SST reconstruction based on ICOADS SST anomalies with a horizontal resolution of 2° × 2° starting from 1854. ERSST is constructed as the sum of low-frequency (LF) and high-frequency (HF) components, while the LF was nonparametrically analyzed using averaging and filtering data over a spatial-temporal region, and the HF was analyzed by fitting the observed HF anomalies (residual anomalies after subtracting the LF components) to a set of large-scale spatial-covariance modes. Satellite data are not used in ERSST v3b as they led to residual biases.

HadISST (Hadley Center Global Sea Ice and Sea Surface Temperature Version 1.1; Rayner et al., 2003): a SST analysis built on an EOF-based Reduced Space Optimal Interpolation (RSOI) technique, using SST observations from ICOADS, the Met Office Marine Data Bank (MDB), and satellite products (1982 onward). Noninterpolated observed SST anomalies were then superimposed onto the reconstructed SST to improve the localized variability. HadISST has a horizontal resolution of 1° × 1° and starts from 1870.

Our study focuses on the time period of 1982–2015, during which all products are available. All seven ocean temperature products are interpolated to a horizontal grid of 1° × 1° using bilinear interpolation and are detrended (removing the quadratic trend of monthly data). The DMI is calculated as the SST anomaly differences between the west (50–70°E, 10°S–10°N) and east (90–110°E, 10°S–0°N) equatorial Indian Ocean. We apply EOF analysis to SON SST anomalies over the tropical Indian Ocean (5°S–5°N and 40–100°E). The anomalies of SST are calculated referencing to the SON climatology of 1982–2015. Given that it is the equatorial nonlinear zonal and vertical advection that is important in driving extreme pIOD, and that an EOF analysis is a mathematical procedure that may not have corresponding physical processes, our EOF analysis domain is intentionally focused on the equatorial region to maximize the correspondence between the mathematical procedure and the nonlinear advection. This is important because later we remove the nonlinear advection and apply the EOF analysis again to show that the nonlinearity between EOF1 and EOF2 is indeed due to the equatorial nonlinear advection.

We have carried out a heat budget of the tropical Indian Ocean in the three ocean-model-based products, which is expressed as follows:

$$\partial T^a/\partial t = -[(u^a\partial T^a/\partial x + \bar{u}\partial T^a/\partial x + u^a\partial \bar{T}/\partial x) + (v^a\partial T^a/\partial y + \bar{v}\partial T^a/\partial y + v^a\partial \bar{T}/\partial y) + (w^a\partial T^a/\partial z + \bar{w}\partial T^a/\partial z + w^a\partial \bar{T}/\partial z)] + Q + residual, \quad (1)$$

where T, u, v, and w are potential temperature, and the zonal, meridional, and vertical ocean current velocities, respectively, averaged over the top 50 m (vertical motion over the top 50 m is represented by w at 50 m). Vertical gradient is calculated as the difference between the average over the top 50 m and temperature at 60 m depth. The heat budget analysis over the upper 50 m has been demonstrated to appropriately describe the variation of SST over the tropical Indian Ocean (Cai et al., 2014, 2018; Ng et al., 2015). Differential operators x, y, z, and t represent the zonal, meridional, and vertical directions, and time, respectively. Superscript "a" and overbar denote anomalous and long-term averaged quantities, respectively. Q is the net surface air-sea heat flux, and "residual" is all other factors not explicitly expressed. We examine the heat budget terms averaged over the developing period of IOD events (August to October, ASO), which contribute most to the mature SST anomalies. All variables in the three products

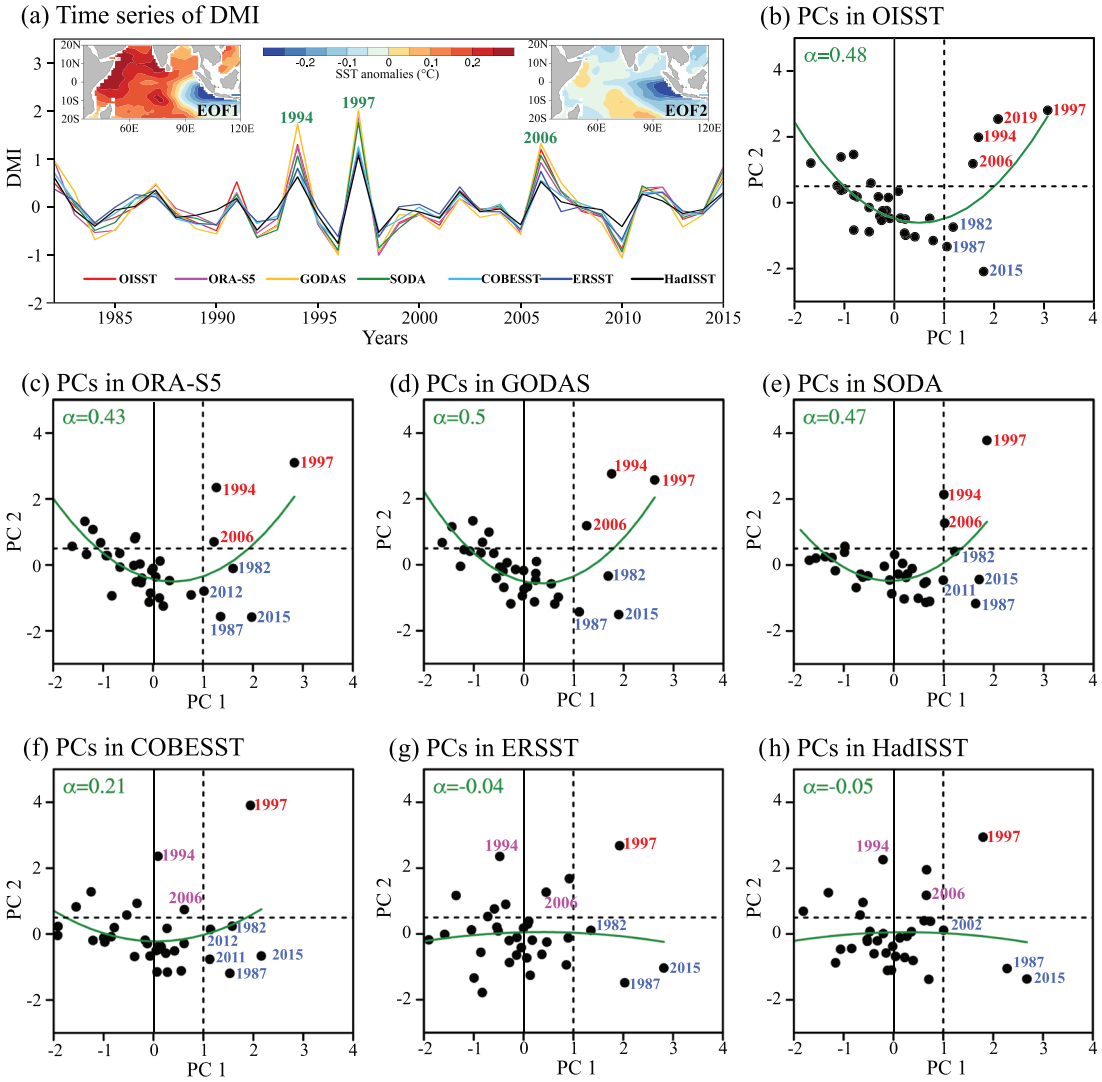

Figure 1. The IOD and depiction of its nonlinearity in seven ocean temperature products. (a) Time series of the DMI (average for the SON) in seven SST products for the period of 1982–2015. Insets: two spatial patterns show SON SST anomalies (°C) regressed onto the first principal component (PC1, left, explains 57% of the total variance on average) and the second principal component (PC2, right, explains 26% of the total variance) of the EOF of SON SST anomalies over the tropical Indian Ocean (5°S to 5°N and 40°E to 100°E) from 1982–2015. SST anomalies are calculated as the mean value of SST anomalies from each of the seven products. (b–h) Nonlinear relationship between the normalized PC1 and PC2 in (b) OISST, (c) ORA-S5, (d) GODAS, (e) SODA, (f) COBESST, (g) ERSST, and (h) HadISST product. The years in red show extreme pIOD years with PC1 > 1 s.d. and PC2 > 0.5 s.d.; the years in blue indicate moderate pIOD years with PC1 > 1 s.d. and PC2 < 0.5 s.d.; the years in purple in (f)–(h) denote the years which are extreme pIOD years in three ocean model-based products (b–e) but not in the non-ocean model-based products (f–h). The green curve shows a nonlinear fit of PC1 and PC2 with a quadratic function $PC2(t) = \alpha[PC1(t)]^2 + \beta PC1(t) + \gamma$. The corresponding value of α is also shown in green. The PC1 and PC2 in 2019 in (b) are obtained by regressing the SON SST anomaly over the tropical Indian Ocean in 2019 from OISST product onto its EOF patterns.

have been interpolated to a horizontal grid of 1° × 1° (bilinear interpolation) and a vertical grid with 5 m interval (linear interpolation) and detrended before calculation.

3. Large IOD Amplitude and Nonlinearity in Ocean Model-Based Products

Although the DMIs in the seven products show high consistency in their variations, a central point that emerges is that OISST and the three ocean model-based products produce larger variability than the three nonocean model-based data, especially for extreme pIOD years, i.e., 1994, 1997, and 2006 (Figure 1a). We perform EOF analysis on the SON SST over the tropical Indian Ocean (5°S–5°N and 40–100°E). As will be

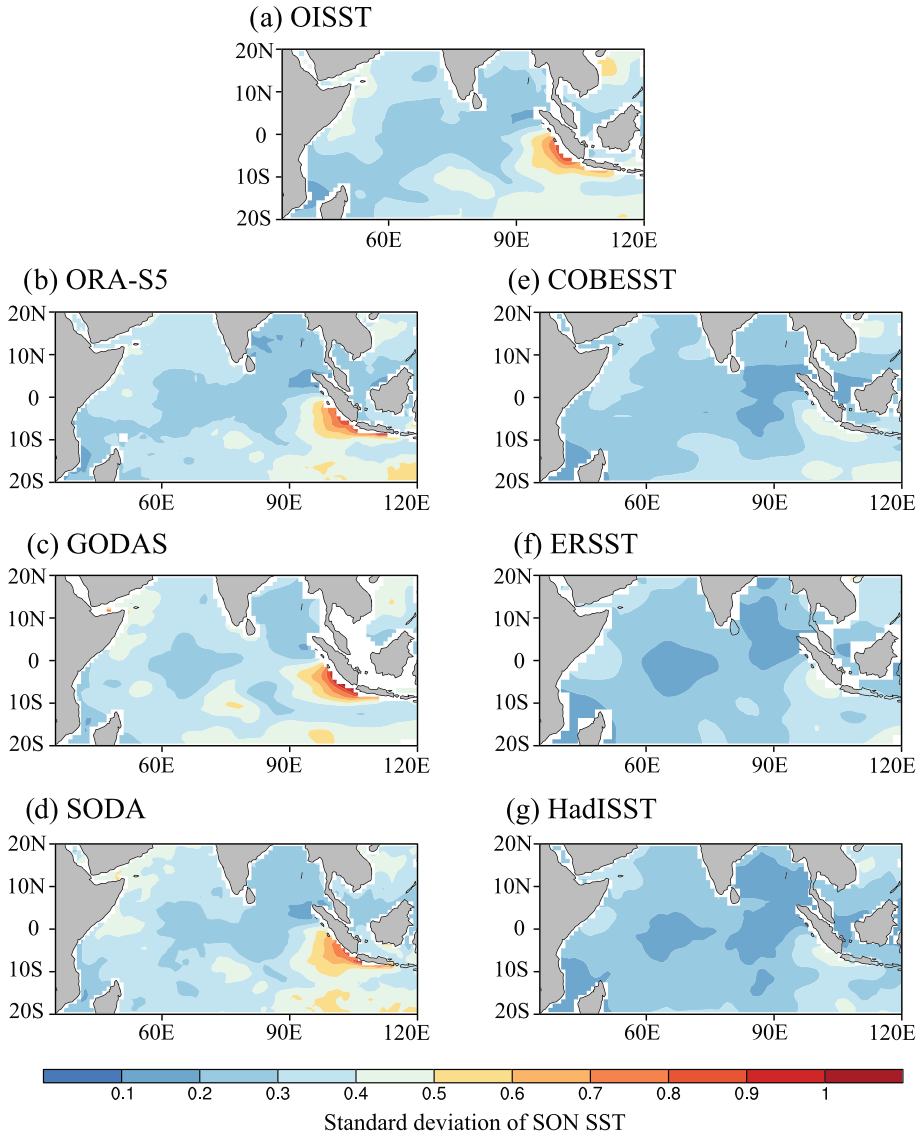

Figure 2. Variability of SON SST anomalies in seven ocean temperature products. (a–g) Spatial distribution of the standard deviation of SON SST anomalies over the tropical Indian Ocean from the (a) OISST, (b) ORA-S5, (c) GODAS, (d) SODA, (e) COBESST, (f) ERSST, and (g) HadISST product.

clear, we focus on the equatorial region, because it is a region where nonlinear processes are dominant. The first and second principal patterns (EOF1 and EOF2, explaining 57% and 26% when applying EOF on average SSTs across products) are generally similar in the seven products (supporting information Figure S1). The EOF1 shows a typical dipole mode pattern, with a cold anomaly center off Sumatra-Java and warm anomalies in the west; the EOF2 generally shows cool anomalies over the equatorial Indian Ocean, with the largest cooling located in the EEIO (inset, Figure 1a).

By definition, EOF analysis yields orthogonal modes such that the first and second principal components (PC1 and PC2) of the EOF modes have a zero correlation, as guaranteed by the mathematical operation. EOF1 reflects the averaged pattern of all IOD events, and the associated PC1 is strongly correlated with the DMI (correlation coefficient of ~0.9).

Importantly, PC1 and PC2 in OISST and the three ocean model-based products display a strong nonlinear relationship, i.e., PC2 is a nonlinear function of PC1, expressed as $PC2(t) = \alpha[PC1(t)]^2 + \beta PC1(t) + \gamma$,

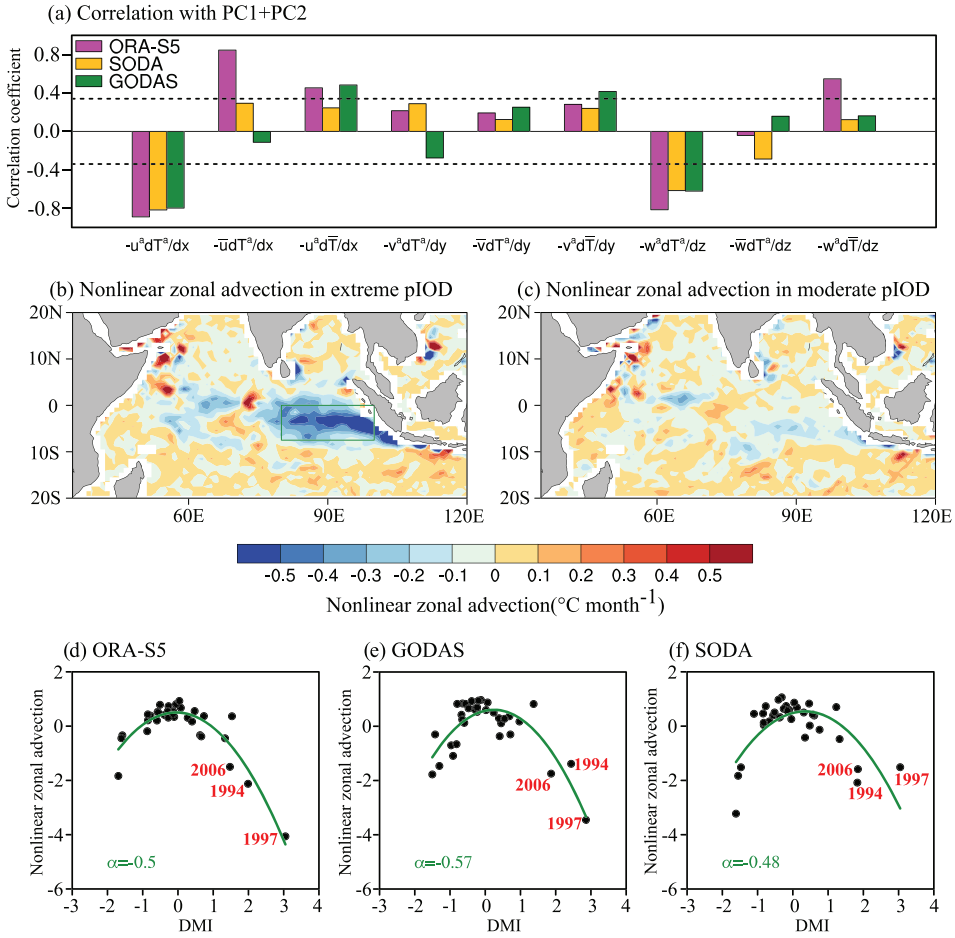

Figure 3. Relationship between the pIOD and heat budget terms. (a) Correlation coefficients between the sum of PC1 and PC2 (which is used describing extreme pIOD events) and the heat budget terms averaged over the tropical Indian Ocean (5°S to 5°N and 40°E to 100°E) in ASO months from the three ocean model-based products for the period of 1982–2015. Black dashed lines show correlation coefficients significant above the 95% confidence level. (b–c) Composite of nonlinear zonal advection term in ASO for (b) extreme pIOD events (1994, 1997, 2006) and (c) moderate pIOD events (1982, 1987, 2015). Nonlinear zonal advection term is from ORA-S5. (d–f) Nonlinear relationships of normalized DMI and area mean nonlinear zonal advection over the 7.5°S to 0°N and 80°E to 100°E area (green box in b) in (d) ORA-S5, (e) GODAS, and (f) SODA. The green curve shows a quadratic fit of the two variables. The corresponding value of α is shown in green. Extreme pIOD events are shown in red.

where α ranges from 0.43 to 0.5 (Figures 1b–1e). This nonlinearity of SST variability is similar to the nonlinearity of rainfall variability in Cai et al. (2014). The nonlinear relationship means that for some pIODs the cold anomalies off Sumatra-Java, where Bjerknes feedback operates, when sufficiently large, i.e., with a large positive PC1, may trigger a set of processes in the EEIO, giving rise to the additional cold anomalies in the EEIO region as shown in EOF2 (Figures 1b–1e). For moderate pIODs, the equatorial processes are weaker and need to be subtracted from the all-event average of EOF1, i.e., as indicated by a negative PC2 (Figures 1b–1e). As will be clear in section 4, this reflects the consequence of nonlinear zonal and vertical advection over the EEIO. In this way, a combination of the two PCs clearly distinguish pIODs into two regimes. One is extreme pIOD, with a threshold of 1 standard deviation (s.d.) for PC1 and 0.5 s.d. for PC2 (Figures 1b–1e). That is, an extreme pIOD event (PC1 > 1 s.d. and PC2 > 0.5 s.d.) is a superimposition of a positive EOF1 and a positive EOF2, with strengthened cooling in the east pole of the IOD. The other regime is moderate pIOD (PC1 > 1 s.d. and PC2 < 0.5 s.d.), which is a combination of a positive EOF1 and a negative (or a weakly positive) EOF2, with weak cold anomalies in the EEIO. In OISST and the three ocean model-based products, 1994, 1997, and 2006 have been identified as extreme

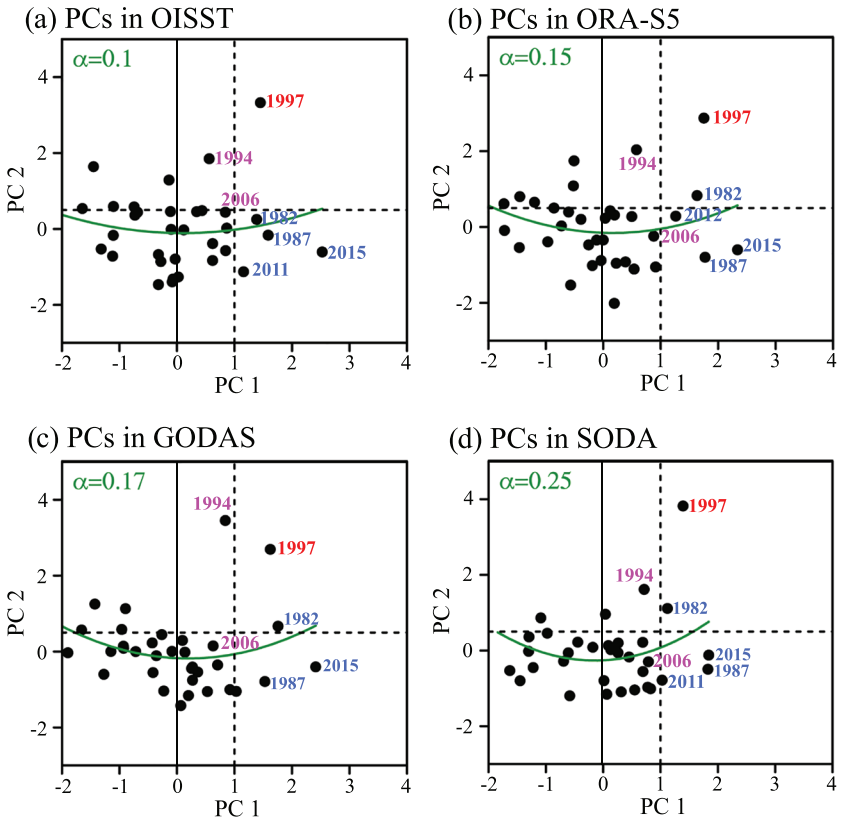

Figure 4. Impact of nonlinear zonal and vertical advection on IOD nonlinearity. Shown is for OISST and the three ocean model-based products after removing anomalies associated with the nonlinear zonal and vertical advection. (a–d) Same as Figures 1b–1e, but with the nonlinear zonal and vertical advection signals removed from the original SON SST in the corresponding products. The heat budget terms used for OISST are calculated from the ORA-S5 data set.

events, while 1982, 1987, and 2015 have been identified as moderate events (Figures 1b–1e). The PC1 value of 1997 in OISST and the three ocean model-based products is large. To see how the 2019 pIOD ranks, we project SON SST anomalies from the OISST product onto its EOF patterns and confirm that the event is an extreme pIOD (Figure 1b).

By contrast, in three non-ocean model-based products, the relationship between PC1 and PC2 is weak, with a small α ranging from −0.05 to 0.21 (Figures 1f–1h). Using the same threshold in Figures 1b–1e, the three products identify similar moderate pIOD events as in Figures 1b–1e, but only find the year 1997 as extreme pIOD event, with a PC1 value smaller than some moderate events. The value of PC1 in 1994, 2006 are small and even negative (Figures 1f–1h). Overall, the three ocean model-based products produce results more similar to those in OISST (Figure 1b). The disparity between products is reflected in SST variability. The OISST and three ocean model-based products generally show larger standard deviation of SST averaged in SON over the tropical Indian Ocean than the other three products, especially near the EEIO and off Sumatra-Java (Figure 2). This means that larger variability of the IOD in OISST and in the three ocean model-based products, compared with that in the other three products (Figure 1a), is related to larger SST variability over the EEIO (Figure 2). The weak SST variability in the three non-ocean model-based products (Figures 2e–2g) is in turn related to their poor ability in capturing the extreme events. Below, we show that the prominent inter-product difference is related to whether the products are generated in a system involving equatorial nonlinear zonal and vertical advection.

4. Equatorial Nonlinear Dynamics Underpins Inter-product Differences

We calculate the heat budget terms at each grid point for the developing phase of the pIOD (ASO) in the three ocean model-based products. The key terms contributing to the extreme events are nonlinear zonal

advection and nonlinear vertical advection (Figure 3a), in agreement with the result of Cai et al. (2014). First, the nonlinear advection (e.g., nonlinear zonal advection) is important for extreme pIOD events and large in the EEIO, consistent with the notion that it is triggered when a large cooling off Sumatra-Java extends to the equatorial region (Figures 3b and 3c). Second, the nonlinear nature, i.e., reinforcing pIOD (cooling in the east) but damping nIOD, is reflected a quadratic function of the DMI or PC1 (Figures 3d–3f).

To confirm that it is the effect of nonlinear zonal and vertical advection on the nonlinearity of the pIOD that accounts for the difference between ocean model-based and non-ocean model-based products, we remove the nonlinear effect and reconduct EOF analysis on the residual anomalies after removal. At each grid point, we add normalized time series of nonlinear zonal and vertical advection in ASO to construct a time series of the combined nonlinear terms. We then regress SON SST anomalies at each grid point onto the time series of the combined nonlinear terms at each grid point. The part of the SST anomalies due to the nonlinear advection is subsequently removed by subtracting the regressed anomalies from the original SST anomalies. For OISST, because there are no subsurface records in OISST, we removed SST anomalies that are associated with nonlinear zonal and vertical advection in ORA-S5. Using those from GODAS, SODA, or those averaged across the three ocean model-based products yields similarly results (Figure S2).

Specifically, after removing the influence from the nonlinear advection, the nonlinear relationship between PC1 and PC2 weakens in each of all three ocean model-based products, with α ranging from 0.15 to 0.25 (Figures 4b–4d). For OISST, the α of the two PCs decreases from 0.48 to 0.1. After removal, the relationship between PC1 and PC2 is similar to that in the three nonocean model-based products (Figures 1f–1h). This result demonstrates the key role of nonlinear zonal and vertical advection in generating the nonlinearity of the pIOD. In turn, this underscores the importance of involving oceanic processes in constructing oceanic temperature products.

5. Discussion and Conclusions

The pIOD is a prominent mode of interannual variability of the equatorial Indian Ocean with significant inter-event differences in nonlinear characteristics. In this study, we have examined the nonlinearity of the extreme pIOD, which is described by a combination of the two leading EOF modes of SON SST over the tropical Indian Ocean, in seven ocean temperature products. The EOF1 pattern features a typical dipole pattern as depicted by the DMI, and the EOF2 is characterized by an equatorial eastern Indian Ocean cooling. Using OISST as an accurate representation of the nonlinearity of the pIOD, we compare the other six ocean temperature products and find that products that involve an ocean model in their construction realistically reproduce the amplitude and nonlinear characteristics of the IOD. A manifestation is a nonlinear relationship between the two EOFs. The dynamics of the second EOF are in turn underpinned by a prominent equatorial Indian Ocean nonlinear zonal and vertical advection, which during an extreme pIOD is additional to the Bjerknes feedback off Sumatra-Java.

This explains why products involving an ocean model, therefore including the nonlinear zonal and vertical advection, realistically capture the dynamics of extreme pIOD. Although we examine many products, not all of them are created equal. Products such as COBESST, ERSST, and HadISST cover a long period, but are constructed using heavy spatial smoothing to fill gaps between sporadic observations. For example, HadISST is generated based on EOFs (Rayner et al., 2003). Those statistical approaches may smear out SST anomalies and underrepresent the oceanic processes. Our results thus emphasize the importance of representing these nonlinear oceanic processes in constructing ocean temperature products, especially for studying the extreme pIOD and its climatic impacts.

Data Availability Statement

The data used in this study can be downloaded from the following websites: OISST (https://psl.noaa.gov/data/gridded/data.noaa.oisst.v2.html); ORA-S5 (http://icdc.cen.uni-hamburg.de/1/projekte/easy-init/easy-init-ocean.html?no_cache=1); SODA (https://www2.atmos.umd.edu/~ocean/index_files); GODAS (https://psl.noaa.gov/data/gridded/data.godas.html); COBESST (https://psl.noaa.gov/data/gridded/data.cobe2.html); ERSST (https://psl.noaa.gov/data/gridded/data.noaa.ersst.v3.html); HadISST (https://www.metoffice.gov.uk/hadobs/hadisst/).

Acknowledgments

This work is supported by the Strategic Priority Research Program of Chinese Academy of Sciences, grant XDB40000000. W.C., G.W., and B.N. are supported by CSHOR and the Earth System and Climate Change Hub of the Australian Government's National Environment Science Program. CSHOR is a joint research Center for Southern Hemisphere Oceans Research between QNLM and CSIRO. G.H. is supported by the National Natural Science Foundation of China (91937302, 41831175), the Strategic Priority Research Program of Chinese Academy of Sciences (XDA20060501). K.Y. is supported by China Postdoctoral Science Foundation (2018M640168), Open Research Fund Program of Key Laboratory of Meteorological Disaster of Ministry of Education (Nanjing University of Information Science and Technology) grant KLME201806, and a scholarship from China Scholarship Council.

References

Abram, N. J., Gagan, M. K., McCulloch, M. T., Chappell, J., & Hantoro, W. S. (2003). Coral reef death during the 1997 Indian Ocean Dipole linked to Indonesian wildfires. *Science*, *301*(5635), 952–955. www.jstor.org/stable/3834840, https://doi.org/10.1126/science.1083841

Anil, N., Ramesh Kumar, M. R., Sajeev, R., & Saji, P. K. (2016). Role of distinct flavours of IOD events on Indian summer monsoon. *Natural Hazards*, *82*(2), 1317–1326. https://doi.org/10.1007/s11069-016-2245-9

Ashok, K., Guan, Z., & Yamagata, T. (2003). Influence of the Indian Ocean Dipole on the Australian winter rainfall. *Geophysical Research Letters*, *30*(15), 1821. https://doi.org/10.1029/2003GL017926

Behera, S. K., Luo, J.-J., Masson, S., Delecluse, P., Gualdi, S., Navarra, A., & Yamagata, T. (2005). Paramount impact of the Indian Ocean Dipole on the East African short rains: A CGCM study. *Journal of Climate*, *18*(21), 4514–4530. https://doi.org/10.1175/JCLI3541.1

Behringer, D., & Xue, Y. (2004). Evaluation of the global ocean data assimilation system at NCEP: The Pacific Ocean. Paper presented at the Proc. Eighth Symp. on Integrated Observing and Assimilation Systems for Atmosphere, Oceans, and Land Surface. https://www.researchgate.net/profile/Yan_Xue2/publication/228856991_Evaluation_of_the_global_ocean_data_assimilation_system_at_NCEP_The_Pacific_Ocean/links/57053bef08ae13eb88b944e4.pdf

Bjerknes, J. (1969). Atmospheric teleconnections from the equatorial Pacific. *Monthly Weather Review*, *97*(3), 163–172. https://doi.org/10.1175/1520-0493(1969)097<0163:ATFTEP>2.3.CO;2

Cai, W., Cowan, T., & Raupach, M. (2009). Positive Indian Ocean Dipole events precondition southeast Australia bushfires. *Geophysical Research Letters*, *36*, L19710. https://doi.org/10.1029/2009GL039902

Cai, W., Santoso, A., Wang, G., Weller, E., Wu, L., Ashok, K., et al. (2014). Increased frequency of extreme Indian Ocean Dipole events due to greenhouse warming. *Nature*, *510*(7504), 254–258. https://doi.org/10.1038/nature13327

Cai, W., Wang, G., Gan, B., Wu, L., Santoso, A., Lin, X., et al. (2018). Stabilised frequency of extreme positive Indian Ocean Dipole under 1.5 °C warming. *Nature Communications*, *9*(1), 1419. https://doi.org/10.1038/s41467-018-03789-6

Carton, J. A., Chepurin, G. A., & Chen, L. (2018). SODA3: A new ocean climate reanalysis. *Journal of Climate*, *31*(17), 6967–6983. https://doi.org/10.1175/JCLI-D-18-0149.1

Du, Y., Cai, W., & Wu, Y. (2013). A new type of the Indian Ocean Dipole since the mid-1970s. *Journal of Climate*, *26*(3), 959–972. https://doi.org/10.1175/JCLI-D-12-00047.1

Endo, S., & Tozuka, T. (2016). Two flavors of the Indian Ocean Dipole. *Climate Dynamics*, *46*(11-12), 3371–3385. https://doi.org/10.1007/s00382-015-2773-0

Feng, M., & Meyers, G. (2003). Interannual variability in the tropical Indian Ocean: A two-year time-scale of Indian Ocean Dipole. *Deep Sea Research Part II: Topical Studies in Oceanography*, *50*(12-13), 2263–2284. https://doi.org/10.1016/S0967-0645(03)00056-0

Hirahara, S., Ishii, M., & Fukuda, Y. (2013). Centennial-scale sea surface temperature analysis and its uncertainty. *Journal of Climate*, *27*(1), 57–75. https://doi.org/10.1175/JCLI-D-12-00837.1

Murtugudde, R., McCreary, J. P. Jr., & Busalacchi, A. J. (2000). Oceanic processes associated with anomalous events in the Indian Ocean with relevance to 1997–1998. *Journal of Geophysical Research*, *105*(C2), 3295–3306. https://doi.org/10.1029/1999JC900294

Ng, B., Cai, W., Walsh, K., & Santoso, A. (2015). Nonlinear processes reinforce extreme Indian Ocean Dipole events. *Scientific Reports*, *5*(1), 11697. https://doi.org/10.1038/srep11697

Page, S. E., Siegert, F., Rieley, J. O., Boehm, H.-D. V., Jaya, A., & Limin, S. (2002). The amount of carbon released from peat and forest fires in Indonesia during 1997. *Nature*, *420*(6911), 61–65. https://doi.org/10.1038/nature01131

Rayner, N. A., Parker, D. E., Horton, E. B., Folland, C. K., Alexander, L. V., Rowell, D. P., et al. (2003). Global analyses of sea surface temperature, sea ice, and night marine air temperature since the late nineteenth century. *Journal of Geophysical Research*, *108*(D14), 4407. https://doi.org/10.1029/2002JD002670

Reynolds, R. W., Rayner, N. A., Smith, T. M., Stokes, D. C., & Wang, W. (2002). An improved in situ and satellite SST analysis for climate. *Journal of Climate*, *15*(13), 1609–1625. https://doi.org/10.1175/1520-0442(2002)015<1609:AIISAS>2.0.CO;2

Saji, N. H., Goswami, B. N., Vinayachandran, P. N., & Yamagata, T. (1999). A dipole mode in the tropical Indian Ocean. *Nature*, *401*(6751), 360–363. https://doi.org/10.1038/43854

Smith, T. M., Reynolds, R. W., Peterson, T. C., & Lawrimore, J. (2008). Improvements to NOAA's historical merged land–ocean surface temperature analysis (1880–2006). *Journal of Climate*, *21*, 2283–2296. https://doi.org/10.1175/2007JCLI2100.1

Ummenhofer, C. C., England, M. H., McIntosh, P. C., Meyers, G. A., Pook, M. J., Risbey, J. S., et al. (2009). What causes southeast Australia's worst droughts? *Geophysical Research Letters*, *36*, L04706. https://doi.org/10.1029/2008GL036801

Verdon-Kidd, D. C. (2018). On the classification of different flavours of Indian Ocean Dipole events. *International Journal of Climatology*, *38*(13), 4924–4937. https://doi.org/10.1002/joc.5707

Wang, G., Cai, W., & Santoso, A. (2017). Assessing the impact of model biases on the projected increase in frequency of extreme positive Indian Ocean Dipole events. *Journal of Climate*, *30*(8), 2757–2767. https://doi.org/10.1175/JCLI-D-16-0509.1

Wang, G., Cai, W., Yang, K., Santoso, A., & Yamagata, T. (2020). A unique feature of the 2019 extreme positive Indian Ocean Dipole event. *Geophysical Research Letters*, *47*, e2020GL088615. https://doi.org/10.1029/2020GL088615

Webster, P. J., Moore, A. M., Loschnigg, J. P., & Leben, R. R. (1999). Coupled ocean–atmosphere dynamics in the Indian Ocean during 1997–98. *Nature*, *401*(6751), 356–360. https://doi.org/10.1038/43848

Yu, L., & Rienecker, M. M. (1999). Mechanisms for the Indian Ocean warming during the 1997–98 El Niño. *Geophysical Research Letters*, *26*(6), 735–738. https://doi.org/10.1029/1999GL900072

Zuo, H., Balmaseda, M. A., Tietsche, S., Mogensen, K., & Mayer, M. (2019). The ECMWF operational ensemble reanalysis–analysis system for ocean and sea ice: A description of the system and assessment. *Ocean Science*, *15*(3), 779–808. https://www.ocean-sci.net/15/779/2019/, https://doi.org/10.5194/os-15-779-2019